Model-Based Electrochemical Estimation of Lithium-Ion Batteries

Kandler A. Smith, Christopher D. Rahn, and Chao-Yang Wang

Abstract—**A linear Kalman filter based on a reduced order electrochemical model is designed to estimate internal battery potentials, concentration gradients, and state of charge (*SOC*) from external current and voltage measurements. The estimates are compared with results from an experimentally validated one-dimensional nonlinear finite volume model of a 6 Ah hybrid electric vehicle battery. The linear filter gives, to within ~2%, performance in the 30%-70% *SOC* range, except in the case of severe current pulses that draw electrode surface concentrations to near saturation and depletion; however, the estimates recover as concentration gradients relax. With 4 to 7 states, the filter has low order comparable to empirical equivalent circuit models but provides estimates of the battery's internal electrochemical state.**

I. Introduction

MODEL-BASED battery monitoring algorithms enable efficient and reliable integration of batteries into hybrid electric vehicle (HEV) powertrains. Examples include the generalized recursive least squares algorithm of Verbrugge and Koch [1] and the extended Kalman filter algorithm of Plett [2]. Both algorithms use an assumed empirical battery model to predict state of charge (*SOC*) and maximum pulse power available within some fixed, predetermined voltage limits. In pulsed-power applications, fixed current/voltage limits can be overly conservative, particularly for short-duration, high-rate current pulses that give rise to large ohmic voltage perturbations [3]. In the dynamic HEV environment, it is desirable to be able to predict the electrochemical state of the battery—e.g., internal chemical concentrations and potentials—to more accurately estimate the power or energy available from the battery and avoid damage.

For lithium-ion (Li-ion) batteries, the one-dimensional model of Doyle, Fuller, and Newman [4], [5] derived from porous electrode and concentrated solution theory captures relevant solid-state and electrolyte diffusion dynamics and accurately predicts current/voltage response.

Derivation of a dynamic electrochemical model suitable for battery state estimation is complicated, however, by the infinite dimensionality of the underlying partial differential equation (PDE) system. Using spatially discretized PDEs, distributed parameter-type estimation algorithms have been developed for the lead-acid battery [6] and the nickel-metal-hydride battery [7], although with high order (30-100 states) in comparison to equivalent circuit model-based algorithms (2-5 states). Recently, we used a model order reduction technique to derive a low-order Li-ion battery model in state variable form [8], [9] directly from the physical governing equations [4], [5]. Here, we employ that model in a linear state estimation algorithm and validate its internal estimates against an experimentally validated 313th order nonlinear finite-volume model of a 6 Ah HEV battery [10].

II. Model and Filter

A schematic of the 1D battery model is shown in Fig. 1. During discharge, Li ions diffuse to the surface of carbon particles in the negative electrode, where they react and transfer to an electrolyte solution. The positively charged ions travel through the electrolyte solution via diffusion and migration, where they again react and diffuse into metal oxide active material particles. Electrons that are produced in the negative electrode reaction and consumed in the positive electrode reaction are blocked by the electronically insulating separator and instead must travel through an external circuit.

A. Infinite-Dimensional Time Model

The electrochemical model parameters are defined in Table 1. The 1D electrochemical model [4], [5] consists of four PDEs describing the conservation of Li in the solid phase (written for a spherical active material particle with reaction occurring at the surface),

$$\frac{\partial c_s}{\partial t} = \frac{D_s}{r^2}\frac{\partial}{\partial r}\left(r^2 \frac{\partial c_s}{\partial r}\right) \tag{1}$$

$$D_s \left.\frac{\partial c_s}{\partial r}\right|_{r\ R_s} = \frac{-j^{Li}}{a_s F}, \tag{2}$$

the conservation of Li in the electrolyte phase,

$$\frac{\partial(\varepsilon_e c_e)}{\partial t} = \frac{\partial}{\partial x}\left(D_e \frac{\partial}{\partial x} c_e\right) + \frac{1 - t_+^o}{F} j^{Li} \tag{3}$$

Manuscript received January 15, 2008. This work was performed at the Pennsylvania State University Electrochemical Engine Center and Pennsylvania Transportation Institute and was supported in part by the U.S. Department of Energy Graduate Automotive Technology Education Program.

K. A. Smith was with the Pennsylvania State University, University Park, PA 16802 USA. He is now with the National Renewable Energy, Golden, CO 80401 USA (phone: 303-275-4423; fax: 303-275-4415; e-mail: kandler_smith@ nrel.gov).

C. D. Rahn is Professor of Mechanical Engineering with the Pennsylvania State University, University Park, PA 16802 USA (e-mail: cdrahn@psu.edu).

C.-Y. Wang is Distinguished Professor of Mechanical Engineering with the Pennsylvania State University, University Park, PA 16802 USA (e-mail: cxw31@psu.edu).

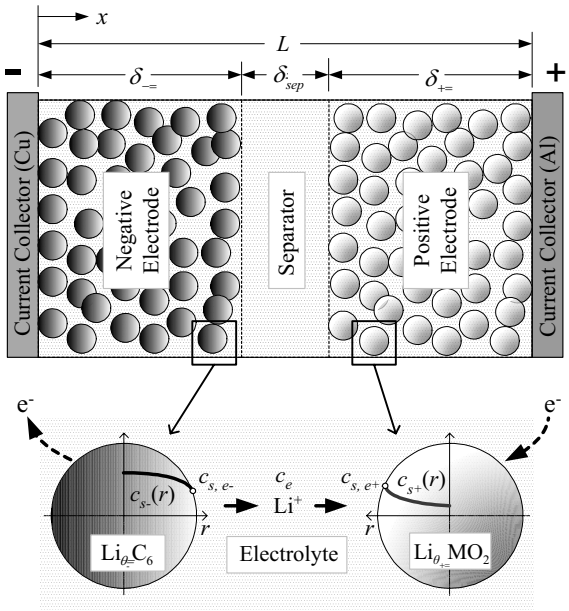

Fig. 1. Schematic of Li-ion battery during discharge.

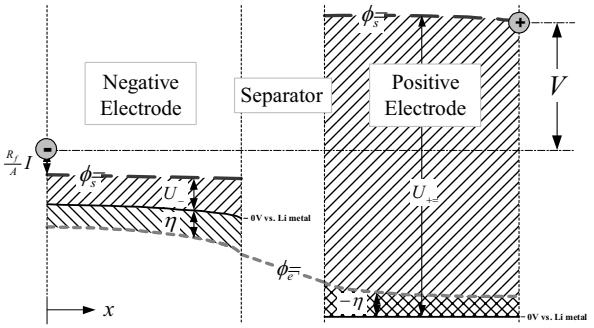

Fig. 2. Schematic of potential gradients across 1D Li-ion battery during discharge.

$$\left.\frac{\partial c_e}{\partial x}\right|_{x\ 0} = \left.\frac{\partial c_e}{\partial x}\right|_{x\ L} = 0, \tag{4}$$

the conservation of charge (e^-) in the solid phase (active material particle/binder matrix),

$$\frac{\partial}{\partial x}\left(\sigma^{-}\frac{\partial \phi_s^{-}}{\partial x}\right) - j^{Li} = 0 \tag{5}$$

$$-\sigma^{-}\left.\frac{\partial \phi_s^{-}}{\partial x}\right|_{x\ 0} \quad \sigma^{-}\left.\frac{\partial \phi_s^{-}}{\partial x}\right|_{x\ L} = \frac{I(t)}{A}, \tag{6}$$

and the conservation of charge in the electrolyte phase,

$$\frac{\partial}{\partial x}\left(\kappa^{-}\frac{\partial \phi_e^{-}}{\partial x}\right) + \frac{\partial}{\partial x}\left(\kappa_D^{-}\frac{\partial \ln c_e}{\partial x}\right)^{-} + j^{Li} \quad 0 \tag{7}$$

$$\left.\frac{\partial \phi_e^{-}}{\partial x}\right|_{x\ 0} = \left.\frac{\partial \phi_e^{-}}{\partial x}\right|_{x\ L} \quad 0 \cdot \tag{8}$$

The four PDEs are coupled by the Butler-Volmer equation describing the reaction current at the solid/electrolyte interface,

TABLE I
ELECTROCHEMICAL MODEL PARAMETERS

Symbol	Description	Units
a_s	electrode specific surface area	cm^2/cm^3
A	electrode plate area	cm^2
c	concentration of Li in a phase	mol/cm^3
D	diffusion coefficient of Li	cm^2/s
F	Faraday's constant	96487 A s/mol
I	current applied at battery terminals	A
i_o	exchange current density of an electrode reaction	A/cm
j^{Li}	reaction current	A/cm^3
Q	battery capacity	A s
R	universal gas constant	8.3143 J/mol K
R_{ct}	linearized charge transfer resistance	$\Omega\ cm^2$
R_s	radius of active material particles	cm
t^o_{+-}	transference number of Li^+ with respect to velocity of solvent	
U	equilibrium potential of an electrode reaction	V
V	voltage at battery terminals	V
ε^-	volume fraction of a phase	
η^-	overpotential of an electrode reaction	V
κ^-	Li^+ conductivity of electrolyte	$1/\Omega$ cm
κ_D	Li^+ diffusional conductivity of electrolyte	A/cm
θ^-	electrode stoichiometry	
σ^-	e^- conductivity of electrode solid matrix	$1/\Omega$ cm
ϕ	phase potential	V
Subscripts		
e	electrolyte phase	
s	solid phase	
s,e	solid phase, at electrolyte interface	
$s\text{-}e$	solid/electrolyte phase difference	
max	maximum in phase	
$-$	negative electrode region	
sep	separator region	
$+$	positive electrode region	
0%	0% state of charge reference	
100%	100% state of charge reference	

$$j^{Li} = a_s i_o\left\{\exp\left[\frac{\alpha_a^{-}F}{RT}\eta\right]^{-} - \exp\left[-\frac{\alpha_c^{-}F}{RT}\eta\right]\right\}^{-}, \tag{9}$$

as a function of overpotential,

$$\eta \quad \phi_s^{-} - \phi_e^{-} - U\,. \tag{10}$$

In (10), note that the phase potential difference must overcome an electrode equilibrium potential $U=U(c_{s,e})$ in order to drive the reaction current in (9). Voltage measured at the battery terminals,

$$V(t) \quad \phi_s^{-}(L,t) - \phi_s^{-}(0,t) - \frac{R_f}{A}I(t), \tag{11}$$

includes an empirical contact resistance between the electrode and current collector.

Fig. 2 provides a schematic of potential gradients internal to the 1D battery during discharge. Under sustained discharge, $I < 0$, all gradients reduce the electromotive force $V(t)$ of the battery. At complete equilibrium (which may take

hours to achieve following even a brief discharge or charge event), $\eta \quad \Delta\phi_e \quad \Delta c_s \quad \Delta c_e \quad 0$, and (11) reduces to the so-called open-circuit voltage,

$$V_{OC} \quad U_+(c_{s,avg+}) - U_-(c_{s,avg-}), \tag{12}$$

Which, alternatively, can be expressed solely as a function of battery *SOC* using conservation relationships.

Lumping each electrode and applying (solid-phase) Li and charge conservation provides a linear relationship between the negative and positive electrode-averaged concentrations,

$$I(t) \quad -\delta_- \varepsilon_{s-} AF \frac{dc_{s,avg-}}{dt} \quad -\delta_+ \varepsilon_{s+} AF \frac{dc_{s,avg+}}{dt}, \tag{13}$$

valid at all times. For estimation purposes, the electrode-averaged concentrations are normalized and written as a linear function of *SOC,*

$$c_{s,\mathrm{avg}}(t) \quad \left[SOC(t)\left(\theta_{100\%} - \theta_{0\%}\right) + \theta_{0\%}\right] c_{s,\max}, \tag{14}$$

where $\theta_{0\%}$ and $\theta_{100\%}$ are the reference stoichiometries of each electrode at 0% and 100% *SOC*, respectively. Note that, by substituting the time derivative of (14) into (13), one recovers the ampere-hour integration-type definition of *SOC* more commonly found in the estimation literature,

$$I(t) \quad -\frac{1}{Q}\frac{d(SOC)}{dt}, \tag{15}$$

where $Q \quad \delta\varepsilon_s AFc_{s,\max}\left|\theta_{100\%} - \theta_{0\%}\right|$ is the usable capacity of each electrode, equivalent to the battery capacity.

B. Infinite-Dimensional Impedance Model

As the first step in model order reduction [11], transfer function/matrix solutions are derived with current as input and electrochemical field variables as output. Solutions for individual field variables are then combined to predict battery voltage.

The solid-state diffusion impedance of a spherical electrode active material particle is [12]

$$\frac{\bar{c}_{s,e}(s)}{\bar{j}^{Li}(s)} \quad \frac{1}{a_s F}\left(\frac{R_s}{D_s}\right)\begin{bmatrix} \tanh(\beta) \\ \tanh(\beta) - \beta \end{bmatrix}, \tag{16}$$

where $\beta = R_s\sqrt{s/D_s}$, and the overbars indicate Laplace transformed variables. Dimensionless impedance $\nu(s)$ of an electrode is [13]

$$\nu(s) \quad \delta\left(\frac{1}{\kappa} + \frac{1}{\sigma}\right)^{\frac{1}{2}}\left(\frac{R_{ct}}{a_s} + \frac{\partial U}{\partial c_s}\left(\frac{\bar{c}_{s,e}(s)}{\bar{j}^{Li}(s)}\right)\right)^{-\frac{1}{2}}. \tag{17}$$

In the present work, equilibrium potential $U(c_{s,e})$ and charge transfer resistance $R_{ct} \approx \eta / j^{Li}$ are both linearized at the 50% *SOC* rest condition.

We define the dimensionless electrode position $z = x / \delta$, where $z = 0$ is the current collector interface and $z = 1$ is the separator interface. For current $I(t)$ applied at the battery terminals, Smith, Rahn, and Wang [8] derive 1D transcendental transfer functions for reaction rate j^{Li},

$$\frac{\bar{j}^{Li}(z,s)}{\bar{I}(s)} \quad \frac{1}{\delta A}\frac{1}{\kappa+\sigma}\frac{\nu(s)}{\sinh\nu(s)} \times \left\{\kappa\cosh\left[\nu(s)(z-1)\right] + \sigma\cosh\left[\nu(s)(z)\right]\right\}, \tag{18}$$

overpotential,

$$\frac{\bar{\eta}(z,s)}{\bar{I}(s)} \quad \frac{R_{ct}}{a_s}\frac{\bar{j}^{Li}(z,s)}{\bar{I}(s)}, \tag{19}$$

electrode bulk-to-surface concentration difference $\Delta c_{s,e} = c_{s,e} - c_{s,avg}$,

$$\frac{\Delta\bar{c}_{s,e}(z,s)}{\bar{I}(s)} \quad \frac{\bar{c}_{s,e}(s)}{\bar{j}^{Li}(s)}\frac{\bar{j}^{Li}(z,s)}{\bar{I}(s)} - \frac{\bar{c}_{s,\mathrm{avg}}(s)}{\bar{I}(s)}, \tag{20}$$

and electrode bulk concentration $c_{s,avg}$,

$$\frac{\bar{c}_{s,\mathrm{avg}}(s)}{\bar{I}(s)} \quad -\frac{1}{\delta A\varepsilon_s F}\frac{1}{s}. \tag{21}$$

Equations (18)-(21) are written for the negative electrode and are derived under the assumption of uniform electrolyte concentration. For the positive electrode, one can multiply the right-hand sides of (18)-(21) by –1.

Analytical solutions for electrolyte concentration and potential are unduly cumbersome. Spatial discretization of (3) and (4) followed by Laplace transformation yields the transfer matrix

$$\frac{\bar{\mathbf{c}}_e(s)}{\bar{I}(s)} \quad (\mathbf{K}_{c_e} + s\mathbf{M}_{c_e})^{-1}\mathbf{F}_{c_e}\frac{\bar{\mathbf{j}}^{Li}(s)}{\bar{I}(s)}. \tag{22}$$

In (22), $\mathbf{K}_i$, $\mathbf{M}_i$ and $\mathbf{F}_i$ are the stiffness, mass, and forcing matrices defined by the finite element method, and $\bar{\mathbf{c}}_e(s)$ and $\bar{\mathbf{j}}^{Li}(s)$ are n x 1 vectors representing field variables $\bar{c}_e(x,s)$ and $\bar{j}^{Li}(x,s)$ at discrete node points x_i. Similar treatment of (7) and (8) yields the transfer matrix

$$\frac{\Delta\bar{\boldsymbol{\varphi}}_e(s)}{\bar{I}(s)} \quad (\mathbf{K}_{\phi_e^\kappa})^{-1}\left(\mathbf{K}_{\phi_e^{\kappa_D}}\frac{\bar{\mathbf{c}}_e(s)}{\bar{I}(s)} + \mathbf{F}_{\phi_e}\frac{\bar{\mathbf{j}}^{Li}(s)}{\bar{I}(s)}\right), \tag{23}$$

where the first vector element representing $\phi_e(0,s)$ is fixed at zero.

The complete current/voltage impedance model is

$$\begin{aligned}\frac{\bar{V}(s)}{\bar{I}(s)} \quad & \frac{1}{AF}\left(\frac{\partial U_+}{\partial c_{s+}}\frac{1}{\delta_+\varepsilon_{s+}} - \frac{\partial U_-}{\partial c_{s-}}\frac{1}{\delta_-\varepsilon_{s-}}\right)\frac{1}{s} \\ & - \frac{\frac{\partial U_-}{\partial c_{s-}}\Delta\bar{c}_{s,e}(0,s) + \bar{\eta}(0,s) - \Delta\bar{\phi}_{e-}^{j^{Li}}(0,s)}{\bar{I}(s)} \\ & + \frac{\frac{\partial U_+}{\partial c_{s+}}\Delta\bar{c}_{s,e}(L,s) + \bar{\eta}(L,s) + \Delta\bar{\phi}_{e+}^{j^{Li}}(L,s)}{\bar{I}(s)} \\ & + \frac{\Delta\bar{\phi}_e^{c_e}(L,s)}{\bar{I}(s)} - \frac{R_f}{A}\end{aligned} \tag{24}$$

with separate terms related to *SOC* dynamics, negative electrode solid diffusion dynamics, positive electrode solid diffusion dynamics, electrolyte diffusion dynamics, and contact resistance static impedance, respectively.

C. Reduced-Order State Variable Realization

Following the procedure in [11], given full order transfer matrix $\bar{\mathbf{y}}(s)/\bar{u}(s)$, the reduced-order transfer matrix is defined as

$$\frac{\bar{\mathbf{y}}^*(s)}{\bar{u}(s)} \quad \mathbf{z} + \sum_{k\ 1}^{n}\frac{\mathbf{r}_k\ s}{s - p_k}, \tag{25}$$

with steady-state vector $\mathbf{z}$ obtained from the full-order model as $\mathbf{z} \lim_{s\to 0} \bar{\mathbf{y}}(s)/\bar{u}(s)$, and poles p_k and residue vectors $\mathbf{r}_k$ numerically generated by minimizing the cost function

$$J \sum_{k=1}^{m}\sum_{i=1}^{n} \left|\mathrm{Re}\left(\bar{\mathbf{y}}_i^*(j\omega_k)-\bar{\mathbf{y}}_i(j\omega_k)\right)\right|^2 + \left|\mathrm{Im}\left(\bar{\mathbf{y}}_i^*(j\omega_k)-\bar{\mathbf{y}}_i(j\omega_k)\right)\right|^2 \quad (26)$$

across the frequency range $\omega \in [0, 2\pi f_c]$, where f_c is the model cutoff frequency. The reduced-order single-input, multiple-output (SIMO) state variable model,

$$\begin{aligned} \dot{\mathbf{x}} &\quad \mathbf{A}\mathbf{x}+\mathbf{B}u \\ \mathbf{y}^* &\quad \mathbf{C}\mathbf{x}+\mathbf{D}u+\mathbf{y}_0 \end{aligned}, \quad (27)$$

is constructed with

$$\mathbf{A} \quad diag[\lambda_1 \cdots \lambda_n], \quad \mathbf{B} \quad [1\cdots 1]^{\mathrm{T}}, \quad \mathbf{C} \quad [\mathbf{r}_1\lambda_1 \cdots \mathbf{r}_n\lambda_n], \quad \mathbf{D} \quad \left[\mathbf{z}+\sum_{k=1}^{n}\mathbf{r}_k\right], \quad (28)$$

eigenvalues $p_k = \lambda_k$, and static constant $\mathbf{y}_0$ giving output $\mathbf{y}^*$ the proper value at the linearization point. In the following, we drop the * symbol from the reduced model for brevity.

The model order reduction procedure requires transfer functions to have finite steady state, a condition satisfied by each of the infinite-dimensional diffusion terms of the voltage/current model, i.e., terms two through five of (24). The first term of (24), related to *SOC*, has a single eigenvalue at the origin and is not reduced. Grouping bulk solid concentration dynamics further into the single *SOC* term is necessary to make the linear model observable.

In [8], the voltage/current state variable model was constructed by separately fitting transfer functions for negative electrode solid diffusion, positive electrode solid diffusion, and electrolyte diffusion dynamics giving model states $\mathbf{x} = [SOC\ \mathbf{x}_-^T\ \mathbf{x}_+^T\ \mathbf{x}_e^T]^T$. In cases in which eigenvalues for the negative and positive electrode states are closely matched, however, we find that positive and negative electrode diffusion dynamics may share the same set of eigenvalues, $\boldsymbol{\lambda}_\pm$, with little loss in accuracy. Taking this approach, model states are $\mathbf{x} = [SOC\ \mathbf{x}_\pm^T\ \mathbf{x}_e^T]^T$ in the present work.

D. Kalman Filter

The standard Kalman filter formulation assumes the plant contains process noise w and measurement noise v in the form

$$\begin{aligned} \dot{\mathbf{x}} &\quad \mathbf{A}\mathbf{x}+\mathbf{B}u+\mathbf{G}w \\ y &\quad \mathbf{C}\mathbf{x}+\mathbf{D}u+y_0+v \end{aligned}. \quad (29)$$

State estimates $\hat{\mathbf{x}}$ are calculated from sensor measurements $u(t)$ and $y(t)$ as

$$\dot{\hat{\mathbf{x}}} \quad \mathbf{A}\hat{\mathbf{x}}+\mathbf{B}u+\mathbf{L}(y-y_0-\mathbf{C}\hat{\mathbf{x}}+\mathbf{D}u). \quad (30)$$

The optimal filter gain $\mathbf{L}$ is precalculated offline as a function of process noise covariance $\mathbf{Q}_w$, measurement noise covariance $\mathbf{Q}_v$, and process noise input matrix $\mathbf{G}$ to minimize the steady-state error covariance

$$\mathbf{P} \quad \lim_{t\to\infty} E\left([\mathbf{x}-\hat{\mathbf{x}}][\mathbf{x}-\hat{\mathbf{x}}]^T\right). \quad (31)$$

III. Results and Discussion

In previous work, we identified and validated a 313th order nonlinear finite-volume model solving (1)-(11) against constant current, transient pulse current, and driving cycle experimental data from a 6 Ah Li-ion HEV battery [10]. In this work, we derive the Kalman filter based on the reduced-order SIMO model (27) and simulate the response using the finite-volume model (see [10] for model parameters).

For the reduced-order model, we use 5 states to describe positive and negative electrode solid-state concentration gradient dynamics and 1 state to describe electrolyte concentration gradient dynamics. This $5D_{s\pm}/1D_e$ state variable model, with 0 to 10 Hz bandwidth, has eigenvalues

$\lambda_{SOC} = 0$,
$\lambda_\pm = -[0.00704, 0.0606, 0.613, 6.10, 63.1]$,
$\lambda_e = -0.0992$ rad/s.

Sizing the filter gain $\mathbf{L}$ requires selection of $\mathbf{Q}_w$, $\mathbf{Q}_v$, and $\mathbf{G}$. To simplify this choice, we interpret w as current sensor noise and adjust its influence on individual states with $\mathbf{G}$. With this interpretation, $\mathbf{Q}_w$ is current sensor noise covariance and $\mathbf{Q}_v$ is voltage sensor noise covariance; here, $\mathbf{Q}_w = (2\mathrm{A})^2$ and $\mathbf{Q}_v = (0.025\mathrm{V})^2$. In theory, the relative influence of process noise on individual states may be adjusted with individual elements of $\mathbf{G}$. In the present application, however, we find that filter eigenvalues (eigenvalues of $\mathbf{A}$-$\mathbf{LC}$) deviate very little from model eigenvalues (eigenvalues of $\mathbf{A}$) irrespective of $\mathbf{Q}_w$, $\mathbf{Q}_v$, and $\mathbf{G}$ with the exception of λ_{SOC}. The *SOC* eigenvalue, located at the origin in the open-loop model, takes on negative real values in the closed-loop filter. Attempts to move other filter eigenvalues to slightly faster locations (as little $1.01\cdot\lambda_\pm$) through pole placement causes state estimates to become overly sensitive to sensor noise.

Fig. 3 compares filter results to data generated by the nonlinear finite-volume model simulating a Federal Urban Driving Schedule (FUDS) cycle for a hybrid electric mid-sized passenger car [10] at 50% *SOC*. The cycle consists of short-duration, low-to-medium-rate discharge and charge current pulses for which battery response is largely linear. The sign convention for battery current is $I > 0$ during discharge and $I < 0$ during charge. The current profile, Fig. 3a, is input to the nonlinear finite volume model to simulate the battery's voltage response, Fig. 3b. These current and voltage "measurements" are played through the filter to generate estimates shown in Fig. 3c-e. Filter states are initialized at $\hat{\mathbf{x}}(0) = [0.2\ \ 0\ \ldots\ 0]^T$, i.e., 20% *SOC* with zero solid and electrolyte phase concentration gradients. The filter gain is sized with $\mathbf{G} = [0.005\ \ldots\ 0.005]$, giving 20-30 second convergence to proper *SOC* (Fig. 3c). Faster converging filters yield noisy estimates when sensor noise is included in the simulation. To simplify discussion, Fig. 3d and Fig. 3e present solid phase surface concentration

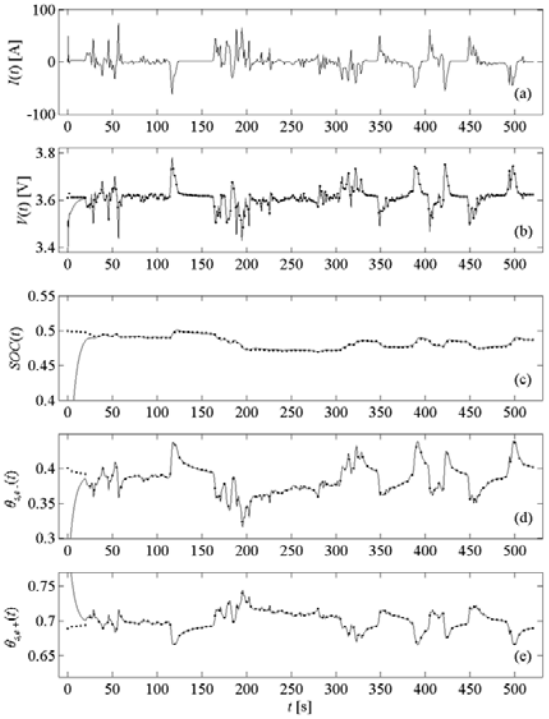

Fig. 3. FUDS driving cycle simulation: Nonlinear finite-volume model with 50% *SOC* initial condition (•) and linear filter with 20% SOC initial condition (-); (a) current profile, (b) voltage response, (c) *SOC*, (d) negative electrode average surface stoichiometry, and (e) positive electrode average surface stoichiometry.

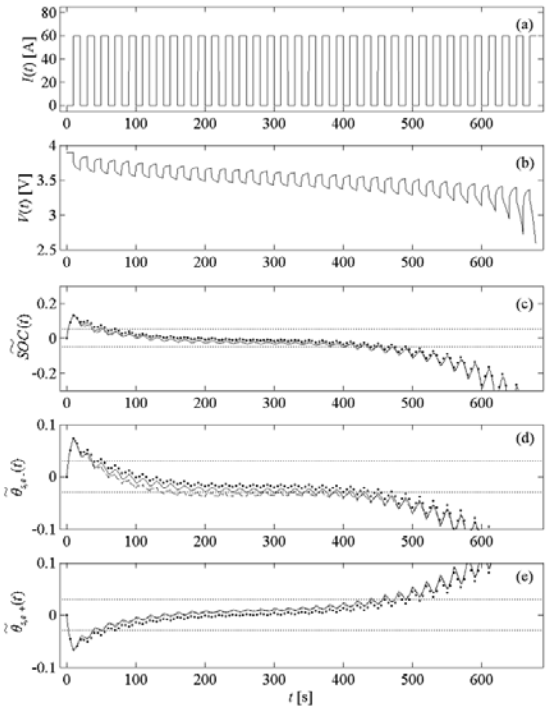

Fig. 5. Ten-second, 60 A pulse discharge profile initiated from 100% *SOC*: (a) current profile; (b) voltage response of nonlinear finite-volume model; (c-e) filter errors: $5D_{s\pm}/1D_e$ (7 state) filter (•), $5D_{s\pm}/0D_e$ (6 state) filter (-), and $3D_{s\pm}/0D_e$ (4 state) filter (--). Horizontal dotted lines denote ±5% *SOC* error threshold in (c) and ±3% surface stoichiometry error thresholds in (d) and (e).

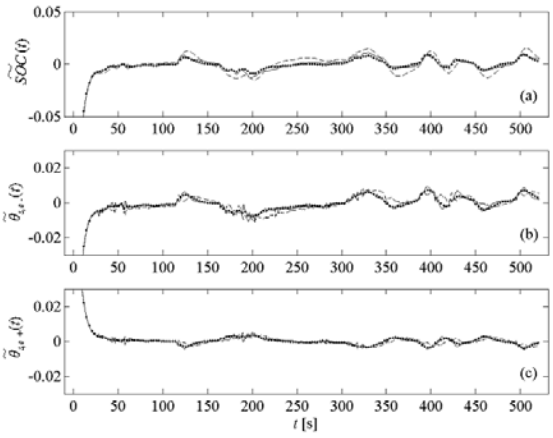

Fig. 4. Filter error for FUDS driving cycle simulation using filters of various order: $5D_{s\pm}/0D_e$ (6 state) filter (•), $4D_{s\pm}/0D_e$ (5 state) filter (-), and $3D_{s\pm}/0D_e$ (4 state) filter (--). The *SOC* initial conditions: 50% and 20%, respectively, for a nonlinear finite-volume model and linear filters.

distributions, $c_{s,e}(x,t)$, as electrode-averaged surface stoichiometries,

$$\theta_{s,e}(t) \quad \frac{1}{\delta \varepsilon_{s,\max}} \int_0^{\delta} c_{s,e}(x,t)\, dx \cdot \tag{32}$$

Surface stoichiometries rise and fall much faster than *SOC* as they are more closely coupled to recent charge/discharge history. Overshoot in *SOC* and surface stoichiometry can occur when filter states $\hat{\mathbf{x}}_{\pm}$ and/or $\hat{\mathbf{x}}_e$ are initialized to nonzero values but convergence is still obtained in 20-30 seconds.

In many situations, particularly for input currents with a negligible DC component such as the FUDS cycle current profile shown in Fig. 3a, lower order filters provide good performance. Electrolyte diffusion dynamics (the fourth term of (24)), impacting the voltage response of the present battery only for sustained medium-to-high-rate currents, may be dropped from the filter, and electrode transcendental transfer functions may be fit with 3rd and 4th order rational transfer functions rather than 5th order. Fig. 4 compares *SOC* and electrode surface stoichiometry errors for filters constructed from $5D_{s\pm}/0D_e$, $4D_{s\pm}/0D_e$, and $3D_{s\pm}/0D_e$ models. The $4D_{\pm}/0D_e$ model has eigenvalues

$\lambda_{SOC} = 0,\ \lambda_{\pm} = -[0.00828, 0.0127, 2.31, 41.5]$ rad/s,

and the $3D_{s\pm}/0D_e$ model has eigenvalues

$\lambda_{SOC} = 0,\ \lambda_{\pm} = -[0.0116, 0.581, 27.3]$ rad/s.

Very little difference is evident among the three filters' performance on the FUDS cycle.

In Fig. 5, the battery is discharged from 100% *SOC* via 60 A pulses of 10 s duration with 10 s of rest between each pulse. The discharge may be interpreted as a 30 A constant current discharge superposed with ±30 A perturbations. The DC component of the current profile causes an electrolyte concentration gradient to be established after approximately 20 s. Comparison of the $5D_{s\pm}/1D_e$ and the $5D_{s\pm}/0D_e$ filters

shows that an additional 1%-2% in *SOC* error and 1% in $\theta_{s,e}$ error is introduced by dropping electrolyte phase dynamics from the filter. Reducing the electrode model from 5 to 3 states introduces an additional 1% error in $\theta_{s,e-}$ but affects $\theta_{s,e+}$ and *SOC* estimates very little.

The discharge presented in Fig. 5 exhibits significant nonlinearities at the beginning (t < 75s) and the end of discharge (t > 450s), where the linear filter performs poorly. Equilibrium potentials U_+ and U_- are functions of surface stoichiometry or concentration and represent the dominant nonlinearity of the battery. The linear filter performs well if $\theta_{s,e-}$ and $\theta_{s,e+}$ remain within approximately ±0.15 of their 50% *SOC* linearization points. Note that surface stoichiometry, and thus equilibrium potential, will be a function of *SOC* only at rest, in the absence of solid-state concentration gradients. At rest, the linear filter is accurate in the interval 27% < *SOC* < 72%. Under discharge or charge, however, surface dynamics can significantly lead bulk dynamics (i.e., *SOC*) and for the particular pulse discharge case shown in Fig. 4, the filter performs well from 92% *SOC* (t = 75 s) to 49% *SOC* (t = 450 s).

IV. Conclusions

This paper shows how filters with low order (4 to 7 states) can be designed from a fundamental Li-ion battery model to estimate the internal electrochemical state of a battery from external current and voltage measurements. The linear filter, based on a 50% *SOC* linearized model, performs well if electrode surface stoichiometries stay within rest values corresponding to 30% to 70% *SOC*. During discharge or charge, however, electrode surface dynamics can significantly lead bulk (*SOC*) dynamics, and a severe discharge/charge event may cause a nonlinear voltage response even with *SOC* near the 50% linearization point. Following such an event, the linear filter recovers as electrode solid-state concentration gradients relax.

Unlike previous electrochemical models formulated using spatial discretization techniques, the present reduced-order model enjoys a computational efficiency comparable to that of equivalent circuit models, a requirement for practical implementation of on-board embedded controllers. Future work should address nonlinear model identification and formulate robust and/or adaptive filters capable of sensing and accounting for battery degradation.

References

[1] M. W. Verbrugge and B. J. Koch, "Generalized recursive algorithm for adaptive multiparameter regression," *J. Electrochemical Soc.*, vol. 153, pp. A187-201, 2006.

[2] G. L. Plett, "Extended Kalman filtering for battery management systems of LiPB-based HEV battery packs—Part 3. State and parameter estimation," *J. Power Sources*, vol. 134, pp. 277-292, 2004.

[3] G. M. Ehrlich, "Lithium ion batteries," in *Handbook of Batteries*, 3rd ed., New York: McGraw-Hill, 2002, pp. 35.53-35.59.

[4] M. Doyle, T. Fuller, and J. Newman. "Modeling of galvanostatic charge and discharge of the lithium/polymer/insertion cell," *J. Electrochemical Soc.*, vol. 140, pp. 1526-1533, 1993.

[5] T. Fuller, M. Doyle, and J. Newman, "Simulation and optimization of the dual lithium ion insertion cell," *J. Electrochemical Soc.*, vol. 141, pp. 1-10, 1994.

[6] A. Tenno, R. Tenno, and T. Suntio, "Charge-discharge behaviour of VRLA batteries: model calibration and application for state estimation and failure detection," *J. Power Sources*, vol. 103, pp. 42-53, 2001.

[7] O. Barbarisi, F. Vasca, and L. Glielmo. "State of charge Kalman filter estimator for automotive batteries," *Control Eng. Practice*, vol. 14, pp. 267-275, 2006.

[8] K. Smith, C. Rahn, and C.-Y. Wang, "Control oriented 1D electrochemical model of lithium ion battery," *Energy Conversion and Management*, vol. 48, pp. 2565-2578, 2007.

[9] K. Smith, *Modeling, Estimation, and Control of Lithium Ion Batteries*, Ph.D. dissertation, Dept. Mech. & Nuc. Engineering, Pennsylvania State Univ., 2006.

[10] K. Smith and C.-Y. Wang, "Solid-state diffusion limitations on pulse operation of a lithium ion cell for hybrid electric vehicles," *J. Power Sources*, vol. 161, pp. 628-639, 2006.

[11] K. Smith, C. Rahn, and C.-Y. Wang, "Model order reduction of 1D diffusion systems via residue grouping," *ASME J. Dyn. Sys. Meas. & Control*, vol. 130, pp. 011012:1-011012:8, 2008.

[12] T. Jacobsen and K. West, "Diffusion impedance in planar, cylindrical and spherical symmetry," *Electrochem. Acta*, vol. 40, pp. 255-262, 1995.

[13] I. Ong and J. Newman, "Double-layer capacitance in a dual lithium ion insertion cell," *J. Electrochem. Soc.*, vol. 146, pp. 4360-4365, 1999.